ExoMol molecular line lists – XX. A comprehensive line list for H_3^+

Irina I. Mizus,[1] Alexander Alijah,[2] Nikolai F. Zobov,[1] Lorenzo Lodi,[3] Aleksandra A. Kyuberis,[1] Sergei N. Yurchenko,[3] Jonathan Tennyson[3]★ and Oleg L. Polyansky[1,3]

[1]*Institute of Applied Physics, Russian Academy of Sciences, Ulyanov Street 46, Nizhny Novgorod 603950, Russia*
[2]*Groupe de Spectrométrie Moléculaire et Atmosphérique, GSMA, UMR CNRS F-7331, Université de Reims Champagne-Ardenne, France*
[3]*Department of Physics and Astronomy, University College London, London WC1E 6BT, UK*

ABSTRACT

H_3^+ is a ubiquitous and important astronomical species whose spectrum has been observed in the interstellar medium, planets and tentatively in the remnants of supernova SN1897a. Its role as a cooler is important for gas giant planets and exoplanets, and possibly the early Universe. All this makes the spectral properties, cooling function and partition function of H_3^+ key parameters for astronomical models and analysis. A new high-accuracy, very extensive line list for H_3^+ called MiZATeP was computed as part of the ExoMol project alongside a temperature-dependent cooling function and partition function as well as lifetimes for excited states. These data are made available in electronic form as supplementary data to this article and at www.exomol.com.

Key words: molecular data – opacity – astronomical data bases: miscellaneous – planets and satellites: atmospheres.

1 INTRODUCTION

The atomic composition of the Universe is dominated by hydrogen which means that H_3^+, as the stable ionic form of molecular hydrogen, is thought to be important in many diverse astronomical environments where it plays a variety of roles (McCall & Oka 2000; Oka 2006). So far H_3^+ has been observed in the atmospheres of the Solar system gas giants (Drossart et al. 1989; Geballe, Jagod & Oka 1993; Trafton et al. 1993; Miller, Lam & Tennyson 1994), dense molecular clouds (Geballe & Oka 1996; McCall et al. 1999), the diffuse interstellar medium (McCall et al. 1998, 2002) and external galaxies (Geballe et al. 2006; Geballe, Mason & Oka 2015), and more tentatively in the remnants of supernova SN1897a (Miller et al. 1992). Observations of H_3^+ provide a powerful tool for studying the Galactic Centre (Goto et al. 2002, 2008; Oka et al. 2005), where it has been shown that lifetime effects in H_3^+ lead to populating long-lived meta-stable states. A similar mechanism is also important in laboratory studies of H_3^+ (Kreckel et al. 2002, 2004). So far, searches for H_3^+ in the atmosphere of hot Jupiter exoplanets have proved negative (Shkolnik, Gaidos & Moskovitz 2006), while the claimed detection of H_3^+ emission in a protoplanetary disc (Brittain & Rettig 2002) was negated by Goto et al. (2005).

H_3^+, which is rapidly formed from the collision of molecular hydrogen and its ion (H_2^+), has long been thought to be the initiator of

much of interstellar gas-phase chemistry (Watson 1973; Herbst & Klemperer 1973; Tennyson 1995; Oka 2013; Millar 2015). It provides a unique means to monitor cosmic ray ionization rates in the interstellar medium (McCall et al. 2003; Indriolo & McCall 2012). Cooling by H_3^+ is thought to be important for the stability of atmospheres of giant extrasolar planets orbiting close to their stars (Koskinen, Aylward & Miller 2007; Khodachenko et al. 2015) and possibly in primordial gas (Glover & Savin 2006). Cooling is one of a number of functions performed by H_3^+ in the ionospheres of Solar system gas giants (Miller et al. 2000) where observations of H_3^+ have proved important for monitoring the ionospheric activity (Miller et al. 1995, 2000; Lam et al. 1997a,b; Stallard et al. 2008a,b) and have, for example, been used to determine wind speeds (Rego et al. 1999). Elsewhere H_3^+ is probably a key component of cool stars with low metallicity; for example it has been shown to play a crucial role in the chemical evolution of cool white dwarfs (Bergeron, Ruiz & Leggett 1997).

H_3^+ has no known electronic spectrum and its 'forbidden' pure rotational spectrum, although possibly observable (Pan & Oka 1986; Miller & Tennyson 1988b), is yet to be detected. This leaves its vibration–rotation spectrum as the means by which all spectroscopic studies are made. The laboratory spectroscopic data for H_3^+ were recently collected and reviewed by Furtenbacher et al. (2013) as part of their MARVEL, Measured Active Rotational–Vibrational Energy Levels (Furtenbacher, Császár & Tennyson 2007; Furtenbacher & Császár 2012), study of the system. This work replaced an earlier compilation and evaluation of the laboratory data by Lindsay &

McCall ([2001](#)). Furtenbacher et al. ([2013](#)) provide a set of empirical energy levels for H_3^+ which we use below.

Kao et al. ([1991](#)) presented a line list of 699 astronomically important H_3^+ lines based on laboratory transition frequencies and *ab initio* transition intensities. The work was supplemented by Neale, Miller & Tennyson ([1996](#)) (NMT below) who computed a much more extensive H_3^+ line list composed of about 3×10^6 lines. These calculations were based on the use of an empirically determined potential energy surface (PES) (Dinelli, Polyansky & Tennyson [1995](#)) and an *ab initio* dipole moment surface (DMS) (Lie & Frye [1992](#)). The quality of this line list was determined first of all by the high accuracy of the fitted PES used for the calculation of the wavefunctions, leading to a standard deviation with respect to the experimental energy levels of only 0.009 cm^{-1}. One of the reasons of this accuracy was the simultaneous fit of all H_3^+ isotopologues, based on the accurate *ab initio* determination of both symmetric and asymmetric adiabatic surfaces of H_2D^+ and D_2H^+ (Polyansky et al. [1995](#)). Note that only states with energies up to 15 000 cm^{-1} were considered in these studies; indeed, NMT regarded their results for states above the barrier to linearity at about 10 000 cm^{-1} as highly uncertain as at that time there was no available spectroscopic data for H_3^+ probing this region. Neale & Tennyson ([1995](#)) provided a high-temperature partition function for H_3^+ which was significantly larger at high T than some previous functions used by astronomers; they showed that such values relied on considering all the levels up to the dissociation limit of H_3^+ at about 35 000 cm^{-1}. NMT also provided the first H_3^+ cooling function, which was refined in subsequent studies (Miller et al. [2010](#), [2013](#)) also based on the NMT line list.

The NMT line list has been widely used for astronomical and other studies. For example, the use of the NMT line list was instrumental in assignment and reassignment of numerous experimentally observed lines by Dinelli et al. ([1997](#)). It has also been shown to be very accurate for spectroscopic intensity predictions (Pavanello et al. [2012a](#); Petrignani et al. [2014](#)), perhaps surprisingly so. However, improved theoretical modelling of the spectroscopy of H_3^+, discussed below, implies that we are now in a position to compute a line list which is both more accurate and more complete, as well as being able to rectify other known issues with the NMT list. NMT performed nuclear motion calculations in Jacobi coordinates and, as a consequence, their wavefunctions did not possess the full symmetry of the system. This symmetry is important for determining whether a state is ortho or para and hence whether its nuclear-spin statistical weight is 4 or 2. NMT assigned symmetry by hand to a few levels but the vast majority were simply given the average statistical weight of 8/3. The use of lower symmetry meant that many of the Einstein A coefficients computed should actually have been zero by symmetry. Because of this and because their line list was very large by contemporary standards, NMT removed all very weak transitions from their line list. This had the unintended consequence of removing those transitions which allow some long-lived meta-stable states of H_3^+ to decay by photon emission, which in turn limits the use of the NMT data for modelling population trapping in H_3^+ and, by extension, for constructing a reliable low-temperature cooling function. We note that the more recent line list for H_2D^+ computed by Sochi & Tennyson ([2010](#)) does not suffer from these problems.

The present work provides a new line list for H_3^+. Unlike NMT, the model used here is essentially *ab initio*. H_3^+ is a two-electron system and is a benchmark for developments in high-accuracy *ab initio* quantum chemical methods (Röhse et al. [1994](#); Cencek et al. [1998](#); Polyansky & Tennyson [1999](#); Schiffels, Alijah & Hinze [2003a](#),[c](#); Kutzelnigg & Jaquet [2006](#); Pavanello et al. [2009](#), [2012b](#);

Diniz et al. [2013](#)). Of particular note here is the non-adiabatic model developed by Polyansky & Tennyson ([1999](#)) and the ultra-high-accuracy *ab initio* PES of Pavanello et al. ([2012b](#)). Use of these was found to give frequency predictions of outstanding accuracy (Pavanello et al. [2012a](#)). Theory has always played an important part in the astronomical spectroscopy of H_3^+ since, as yet, there is only a single (McKellar & Watson [1998](#)) absolute laboratory measurements of H_3^+ line intensities. However, empirical tests of predicted intensities have also been provided by experiments measuring intensity ratios for transitions with widely differing wavelengths and intensities (Farnik et al. [2002](#); Asvany et al. [2007](#); Petrignani et al. [2014](#)). The most stringent test was provided by the visible-wavelength measurements of Petrignani et al. ([2014](#)) which showed that their DMS, used here, predicted the observed intensities in a very satisfactory manner.

This new H_3^+ line list, which we call MiZATeP, is computed as part of the ExoMol project (Tennyson & Yurchenko [2012](#)) which has provided a large number of molecular line lists for exoplanet and other atmospheres (Tennyson et al. [2016b](#)). The line lists produced by ExoMol to date are summarized in Table [1](#); in addition, the BT2 $H_2^{16}O$ (Barber et al. [2006](#)) and BYTe NH_3 (Yurchenko, Barber & Tennyson [2011](#)) pre-dated the start of the project. H_3^+ is the first molecular ion studied as part of the ExoMol project, although line lists for H_2D^+ (Sochi & Tennyson [2010](#)), HeH$^+$ (Engel et al. [2005](#)), HD$^+$ (Coppola, Lodi & Tennyson [2011](#)) and LiH$^+$ (Coppola et al. [2011](#)) were computed previously.

2 METHOD

Nuclear motion calculations used the highly accurate global *ab initio* PES presented by Pavanello et al. ([2012b](#)) and the related DMS given by Petrignani et al. ([2014](#)). The DMS is expressed in the seven-parameter form of Lie & Frye ([1992](#)) which was found to best reproduce the observations. The calculations were based on the DVR3D program suite (Tennyson et al. [2004](#)) and were performed for two different choices of the basis set and were augmented by a third set of calculations for labelling purposes performed using a separate program by Wolniewicz ([1988](#)).

The bulk of the calculations were performed in Jacobi coordinates and used the Polyansky & Tennyson ([1999](#)) model to allow for non-adiabatic effects. Discrete variable representation (DVR) grids were based on spherical oscillator functions (Tennyson & Sutcliffe [1983](#)) for both the atom–diatom coordinate and diatomic (Tennyson & Sutcliffe [1982](#)) coordinate, and (associated) Legendre functions for the angular coordinate. The grids contained 60, 58 and 68 points for these coordinates, respectively. The final diagonalized matrices for the vibrational problem had a dimension of 20 000. Further increases of these parameters do not lead to significant changes in the resulting energies. These calculations used spherical oscillators with parameters $\alpha = 0.0$ and $\omega_e = 0.07$ atomic units for both radial coordinates. Non-adiabatic effects were taken into account by using different values for the vibrational and the rotational masses in the kinetic energy operator; the vibrational mass was taken to be equal to 1.007537 D_a – an intermediate value between nuclear and atomic masses suggested by Moss ([1996](#)) on the basis of calculations on H_2^+ isotopologues. The proton (nuclear) mass was used for the rotational mass. These calculations yielded energy levels up to at least 25 000 cm^{-1} for J values up to 25. The model used for the calculation has been shown to give an accuracy of about 0.1 cm^{-1} (Pavanello et al. [2012a](#),[b](#)) for all experimentally observed energy levels. The highest energy level lies at about 17 000 cm^{-1}.

Table 1. Data sets created by the ExoMol project and included in the ExoMol data base.

Paper	Molecule	N_{iso}	T_{max}	N_{elec}	N_{lines}[a]	DS name	Reference
I	BeH	1	2000	1	16 400	Yadin	Yadin et al. (2012)
I	MgH	3	2000	1	10 354	Yadin	Yadin et al. (2012)
I	CaH	1	2000	1	15 278	Yadin	Yadin et al. (2012)
II	SiO	5	9000	1	254 675	EJBT	Barton, Yurchenko & Tennyson (2013)
III	HCN/HNC	2[a]	4000	1	399 000 000	Harris	Barber et al. (2014)
IV	CH_4	1	1500	1	9 819 605 160	10to10	Yurchenko & Tennyson (2014)
V	NaCl	2	3000	1	702 271	Barton	Barton et al. (2014)
V	KCl	4	3000	1	1 326 765	Barton	Barton et al. (2014)
VI	PN	2	5000	1	142 512	YYLT	Yorke et al. (2014)
VII	PH_3	1	1500	1	16 803 703 395	SAlTY	Sousa-Silva et al. (2015)
VIII	H_2CO	1	1500	1	10 000 000 000	AYTY	Al-Refaie et al. (2015)
IX	AlO	4	8000	3	4 945 580	ATP	Patrascu, Tennyson & Yurchenko (2015)
X	NaH	2	7000	2	79 898	Rivlin	Rivlin et al. (2015)
XI	HNO_3	1	500	1	6 722 136 109	AIJS	Pavlyuchko, Yurchenko & Tennyson (2015)
XII	CS	8	3000	1	548 312	JnK	Paulose et al. (2015)
XIII	CaO	1	5000	5	21 279 299	VBATHY	Yurchenko et al. (2016)
XIV	SO_2	1	2000	1	1 300 000 000	ExoAmes	Underwood et al. (2016a)
XV	H_2O_2	1	1250	1	20 000 000 000	APTY	Al-Refaie et al. (2016)
XVI	H_2S	1	2000	1	115 530 373	AYT2	Azzam et al. (2016)
XVII	SO_3	1	800	1	21 000 000 000	UYT2	Underwood et al. (2016a)
XVIII	VO	1	5000	13	277 131 624	VOMYT	McKemmish, Yurchenko & Tennyson (2016)
XIX	H_2O	2[b]	3000	1	519 461 789	HotWat78	Polyansky et al. (2016)
XX	H_3^+	1	5000	1	127 542 657	MiZATeP	This work
XXI	NO	6	5000	1	2 281 042	NOname	Wong et al. (2017)
XXII	H_2O	1[b]	5000	1	12 000 000 000	Pokazatel	Polyansky et al. (2017)

Notes. N_{iso} – Number of isotopologues considered.

T_{max} – Maximum temperature for which the line list is complete.

N_{elec} – Number of electronic states considered.

N_{lines} – Number of lines: value is for the main isotope.

[a] A line list for $H^{13}CN/HN^{13}C$ due to Harris et al. (Harris et al. 2008) is also available.

[b] HotWat78 are line lists for $H_2^{18}O$ and $H_2^{17}O$ in the style of the BT2 $H_2^{16}O$ (Barber et al. 2006) and VTT HDO

(Voronin et al. 2010) line lists. Pokazatel, number XXII, is an extended $H_2^{16}O$ line list.

As the PES is *ab initio* we hope that this accuracy extrapolates well to all the energies used in the presented line list.

These DVR3D calculations with big basis were supplemented by second set of smaller calculations which used 31, 31 and 50 grid points for two radial and an angular coordinates, respectively, and with the final vibrational Hamiltonians dimensions equal to 3000. The calculations were performed up to at least 35 000 cm^{-1} and for J values 0–40. Note that the highest bound rotational state for H_3^+ is predicted to have $J = 42$ (Miller & Tennyson 1988a; Jaquet & Carrington 2013). These calculations used Morse-like oscillators (Tennyson & Sutcliffe 1982) with parameters $r_e = 3.1$, $D_e = 0.1$ and $\omega_e = 0.006$ in atomic units for the diatomic radial coordinate and spherical oscillators with parameters $\alpha = 0.0$, and $\omega_e = 0.016$ atomic units for the scattering coordinate. Only nuclear masses were used for these calculations. This set of calculations was performed to achieve better convergence for the partition function and to provide completeness for the final line list by adding transitions to energy states with J values larger than 25. Similar, more approximate treatments of the higher-lying states have been used successfully for other ExoMol line lists and partition sums (Sousa-Silva et al. 2014; Underwood et al. 2016a,b).

Although it is possible to obtain full symmetrization of the DVR3D wavefunctions computed in Jacobi coordinates (Munro, Ramanlal & Tennyson 2005), here we achieved this goal by performing a third set of nuclear motion calculations using the hyperspherical harmonics code of Wolniewicz (1988). The hyperspherical coordinates as defined by Whitten & Smith (1968) and modified by Johnson (1983) are the three internal coordinates consisting of the hyperradius, ρ,

and the two hyperangles θ and ϕ, and the three Euler angles α, β and γ. The symbol Ω is used to collect the five angles, $\Omega = (\theta, \phi, \alpha, \beta, \gamma)$. In these coordinates, the Hamiltonian is written as

$$H(\rho, \Omega) = -\frac{\hbar^2}{2\mu} \left[\frac{1}{\rho^5} \frac{\partial}{\partial \rho} \rho^5 \frac{\partial}{\partial \rho} + \frac{\Lambda^2(\Omega)}{\rho^5} \right] + V(\rho, \theta, \phi), \quad (1)$$

where $\mu = \sqrt{m_1 m_2 m_3 / (m_1 + m_2 + m_3)}$ is the three-particle reduced mass and $\Lambda^2(\Omega)$ the grand angular momentum operator. Its eigenfunctions are the hyperspherical harmonics, $\theta_\alpha^{J\Gamma}(\Omega)$. As shown by Wolniewicz, Hinze & Alijah (1993), they can be symmetrized easily in the three-particle permutation inversion group $S_3 \times I$. The labels are then the total angular momentum J, the symmetry index Γ, and α, a counting index. To solve the rovibrational Schrödinger equation corresponding to Hamiltonian (1), the rovibrational wavefunction is expanded in terms of symmetrized hyperspherical harmonics

$$\Psi_n^{J\Gamma}(\rho, \Omega) = \sum_\alpha \theta_\alpha^{J\Gamma}(\Omega) \frac{P_{\alpha,n}^{J\Gamma}(\rho)}{\rho^{5/2}}. \quad (2)$$

This yields a system of coupled equations in the hyperradius which is integrated numerically. As the expansion converges only slowly, a contracted basis of symmetrized hyperspherical harmonics is used. The contraction coefficients are the lowest eigenvectors obtained from diagonalization of the potential energy matrix, $U(\rho)$, with matrix elements $U_{\alpha,\alpha'}(\rho) = \langle \theta_\alpha^{J\Gamma}(\Omega) | V(\rho, \theta, \phi) | \theta_{\alpha'}^{J\Gamma}(\Omega) \rangle_\Omega$ in the spherical harmonics basis at a ρ value that corresponds to the minimum of the potential, $\rho = 2.21 \, a_0$. The procedure is fully described

by Schiffels, Alijah & Hinze (2003b). Typically, about 1000 primitive hyperspherical harmonics are contracted to 300 basis functions, hence a system of 300 coupled equations is integrated. For each value of J, there are in general six irreducible representations: A'_1, A'_2, E', A''_1, A''_2, E''. Prime representations have even parity, while double prime representations have odd parity. Hence for $J = 0$ there are only three even parity representations.

For the production runs the code was modified so that for each Γ and J the number of basis functions is determined automatically so that, for a given symmetry, only the value of J needs to be set in the input. Numerical integration is done within $0.7\,a_0 \leq \rho \leq 6.2\,a_0$, with a step size of $\Delta\rho = 0.01\,a_0$. The energy range of the desired eigenvalues is split into six parts, and six separate jobs are run to compute the eigenvalues within their respective energy intervals. In the present implementation of the code no eigenfunctions are obtained, which would be needed for the intensity calculations. The DVR3D code was used for this purpose. On the other hand, the hyperspherical code fully exploits permutational symmetry, thus allowing the identification of degenerate states; such degenerate states appear in unsymmetrized DVR3D calculations as a pair of A_1, A_2 states with very similar energy.

The hyperspherical harmonic calculations were used to provide full symmetry labels for states obtained using DVR3D. This labelling procedure was performed for the first set of high-accuracy calculations and was limited to J values up to 20 only. The (quasi-)degenerate even and odd pairs of DVR3D levels which correspond to degenerate f-symmetry levels were identified. These levels are para and have a nuclear-spin degeneracy factor of 2. The degeneracy factor for the A_2-type levels (the unmatched odd levels) is 4. Unmatched even levels are of A_1-type which have zero statistical weight; these levels were discarded.

For higher J we used the procedure suggested by Neale & Tennyson (1995) to set the nuclear-spin degeneracy factor for transitions between energy levels with J values 21–40 in our final line list. This method avoids explicit labelling by using the high-temperature approximation of ascribing a degeneracy factor equal to 8/3 to odd levels, and equal to 0 to even ones. This removes the need to decide if a given pair of levels should be degenerate and therefore of E-type, which becomes increasingly difficult as the calculations are less well converged (Tennyson 1993). Given the small contribution of these high J states, this procedure introduces negligible error in the results given below.

3 LINE LIST CALCULATIONS

A comprehensive line list was calculated for transition frequencies up to 25 000 cm^{-1}. This line list comes in the form of a states file, which stores energy levels and other state-specific information, and a transitions file. Where available, levels from the MARVEL analysis (Furtenbacher et al. 2013) were used to replace our calculated values to ensure the highest possible accuracy.

This new H$_3^+$ line list, which we call MiZATeP, contains transitions between energy states with J values 0–37 and energies 0–42 000 cm^{-1} and consists of 127 542 657 lines with an accuracy close to the spectroscopic one; the 158 721 states considered have rotational quantum numbers up to $J = 37$. On the basis of the calculated energy levels and taking into account their statistical weights we also compute accurate partition and cooling functions, which, we believe, are appropriate for temperatures up to 5000 K. The line list should also be valid up to this temperature. The line list is presented in the updated ExoMol format (Tennyson et al. 2016b);
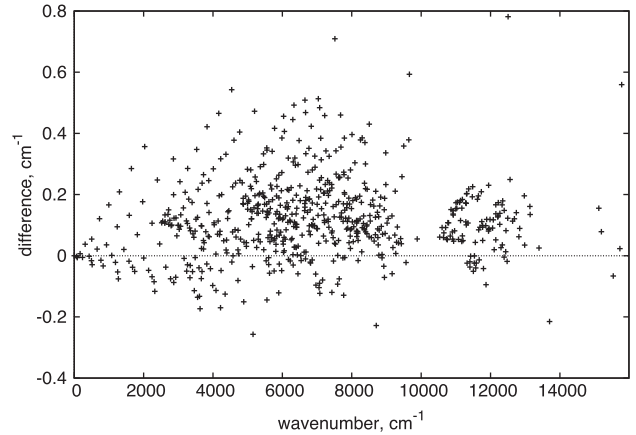
Figure 1. Comparison of our energy levels calculation results with experimental energy values obtained during MARVEL analysis (Furtenbacher et al. 2013).

extracts from the states and transitions files are presented in Tables 5 and 6, respectively.

The energies used in the states file are a mixture: (1) MARVEL energies (Furtenbacher et al. 2013) were used where available; (2) for $J \leq 25$ the high-quality results from the first set of nuclear motion calculations were used; (3) for $J = 26 - 37$ the results of the second set of calculation, performed with the smaller basis set, were used. Levels with $J = 25$ required separate consideration, because transitions between states with $J = 24$ and $J = 25$ (and $25 \longleftrightarrow 25$) are a part of our accurate results, whereas transitions between states with $J = 25$ and $J = 26$ were treated using the results of the calculations with the small basis set. Thus, the states file contains two sets of energy levels with $J = 25$: the accurate ones and the ones obtained within the small basis set. All energy values are given relative to the same highly accurate value of ground state energy. Whenever possible the states have been assigned quantum numbers following the convention of Watson (1984). In particular, the energy of a rovibrational state can be expanded as, according to Watson (1984),

$$E(J, G) = T_0 + BJ(J + 1) + (C - B)G^2 + \cdots \quad (3)$$

where $G = |k - \ell_2|$ and ℓ_2 is the vibrational angular momentum. Since, by convention, $C < B$ holds for the rotational constants, the rotational energy increases, for a given vibrational state and J, with decreasing G. It is reasonable to assume that the states with infinite lifetime (see below) belong to the vibrational ground state and have the largest values of G, i.e. $G \equiv K = J$ and $G \equiv K = J - 1$. We then determine the symmetry of these states, which is A_1/A_2 for $G = 0$, 3, 6, ... (with just one state for $G = 0$) and E for $G = 1, 4, 7, \ldots$ and $G = 2, 5, 8, \ldots$ Prime and double prime labels are according to even or odd parity, respectively, of $G + v_2$. To assign the states in question, we simply pick, of the eigenvalues computed in full symmetry with the hyperspherical harmonics code, the lowest one with the appropriate symmetry. This procedure works, because the lowest rotational levels of the next higher vibrational states, $(0, 1^1)$ and $(1, 0^0)$, are well separated in energy. The tag -1 is used for states for which no approximate quantum number assignments are made.

Fig. 1 shows the result of a comparison of our calculated energy values with almost all available MARVEL energies of states with J values up to 12. Standard deviation between theory and experiment here is about 0.18 cm^{-1}.

Table 2. Comparison of the calculated Einstein's coefficients, *B*, obtained here with the DMS of Petrignani et al. (2014) (B_{calc}), with the experimental data (B_{exp}; Petrignani et al. 2014), and also the results of NMT (B_{NMT}; Neale & Tennyson 1995) and calculations made with DMS of Röhse et al. (1994) on the basis of the PES from Pavanello et al. (2012b) (B_R). *B* values are measured in units 10^{18} cm^3 J^{-1} s^{-2}. The transition frequencies, ν, are taken from the larger DVR3D calculations (see text).

ν (cm^{-1})	B_{exp}	B_{NMT}	B_R	B_{calc}	$\frac{B_{exp}}{B_{NMT}}$	$\frac{B_{exp}}{B_R}$	$\frac{B_{exp}}{B_{calc}}$
7144.005		1550.00	1554.31	1565.21			
10752.085	72.6(16)	60.53	60.297	55.864	1.20	1.20	1.30
10798.626	26.5(30)	32.94	32.964	32.327	0.80	0.80	0.82
10831.526	112(16)	93.98	94.078	96.168	1.19	1.19	1.16
12373.310	4.3(10)	4.040	4.0141	4.5837	1.06	1.07	0.94
12381.054	4.1(10)	4.097	4.0230	4.2277	1.00	1.02	0.97
12413.273	4.6(12)	3.734	3.7896	3.7869	1.23	1.21	1.21
12588.962	1.10(38)	0.8589	0.8599	0.7590	1.28	1.28	1.45
12620.082	6.3(12)	4.858	4.7392	4.4116	1.30	1.33	1.43
12678.540	8.6(17)	8.006	8.0987	8.4727	1.07	1.06	1.02
13332.856*	4.0(13)	2.045	2.0550	1.7871	1.96	1.95	2.24
13638.464	3.9(15)	4.137	4.0570	3.6346	0.94	0.96	1.07
15058.522	1.53(33)	1.6189	1.5916	1.3920	0.95	0.96	1.10
15130.399	0.72(16)	0.7120	0.6979	0.8488	1.01	1.03	0.85
15450.172	0.75(10)	0.7747	0.7716	0.7593	0.97	0.97	0.99
15643.023	1.11(15)	1.0125	1.0103	1.0079	1.10	1.10	1.10
15716.252	1.60(51)	1.3960	1.3802	1.7039	1.15	1.16	0.94
16506.066	1.28(50)		1.1422	1.2165		1.12	1.05
16660.069	0.38(19)		0.4631	0.5872		0.82	0.65

Note. *The assignment of this observed line is doubtful as its intensity is poorly predicted by all theoretical calculations; it was not included in the calculation of standard deviations.

While calculating the final version of our line list, lifetimes, partition and cooling function values, it is only necessary to consider states with odd vibrational symmetry (Tennyson et al. 2004) in the DVR3D calculation; these states include both *E* (one component) and A_2 symmetry states. A_1 states have even symmetry and need not be considered.

Statistical weights were assigned to almost all states with $J \leq 20$ and energies up to 25 000 cm^{-1} through our labelling procedure. These weights are equal to 2 for *E* states and 4 for A_2 states. States outside this range are given the average statistical weight of $g_{ns} = 8/3$. To retain compatibility with the ExoMol format (Tennyson et al. 2016b) for these states, the product $g_{ns} \times (2J+1)$, which gives the total degeneracy of each level, *g*, was rounded to the nearest integer.

The DVR3D program suite for triatomic molecules does not, when using Jacobi coordinates, take into account the symmetry of the system when some of the nuclei are identical, such as in the case of H$_3^+$. As a consequence DVR3D also calculates transitions which are forbidden by the exact H$_3^+$ selection rules, thus producing in the resulting line list many very weak transitions which should actually have zero intensity. We systematically deleted such unwanted transitions from our final line list, but there remains a possibility that there are some allowed but very weak transitions that also got mistakenly deleted due to errors in the labelling procedure.

Intensity calculations were based on the DMS by Petrignani et al. (2014), which has been expanded to an energy region up to 30 000 cm^{-1} to cover all the frequency range needed for our goals. Table 2 presents a comparison of the calculated Einstein *B* coefficients obtained using the DMS of Petrignani et al. (2014), the results of NMT and a new calculation using the DMS of Röhse et al. (1994), with the experimental data from table I of

Petrignani et al. (2014). The standard deviation of the ratio of experimental to calculated values is 22 per cent. The comparison between our calculations with the two DMS suggests that the main source of sensitivity in the intensity calculations is the DMS employed and not the wavefunctions and the underlying PES. The DMS of Petrignani et al. (2014) covers a frequency range about twice as large as the one considered by NMT (Neale et al. 1996), and is only slightly worse in energy region up to 15 000 cm^{-1} – the difference is about 4.5 per cent for the same set of experimental data.

The MiZATeP line list has been compared directly with the NMT one. This comparison shows good coincidence between the two; for example, at room temperature the standard deviation of the ratio of Einstein's A coefficients of the 292 strongest lines (with relative intensity values greater than 0.001) from these line lists is only about 3 per cent.

4 PARTITION FUNCTION AND INTENSITY CALCULATIONS

The labelling procedures described in the previous section were used to assign statistical weights to the line list transitions and for the calculation of the cooling and partition functions. In all these cases we used the second set of nuclear motion calculations, which have comparatively low accuracy, to supplement our high-accuracy levels with levels with energies between 25 000 cm^{-1} and dissociation. This is essential to obtain an accurate partition function at high temperatures. We used the same analytical form for the partition function as Neale & Tennyson (1995).

Our estimates show that the low-accuracy energy levels in the second set of nuclear motion calculations as well as the absence of exact labelling procedure in this case influence the partition function values only slightly: the relative error is less than 10^{-5} for each term in the partition function sum and therefore we can safely ignore this effect.

We computed a number of partition functions. In particular, Q_{37} sums over the levels given in our final states file, which contains levels with $J \leq 37$ and *E* at least up to 35 000 cm^{-1}. Q_{37} is therefore consistent with the associated transitions file. Other partition sums, denoted as Q_J, which summed levels up to *J* and $E \leq 25 000$ cm^{-1}, were also computed. Finally, a partition function computed by summing over all levels for which we calculated energies is denoted as Q_{all}. Q_{all} provides a measure of convergence for the other partition functions which sum over fewer levels.

Table 3 gives our partition function results. It compares our best estimates (Q_{all} and Q_{37}) with value by Neale & Tennyson (1995) and our more approximate sums. While the various values agree well for lower temperatures, our most complete calculations give significantly higher values at high *T*. This suggests that the partition function of H$_3^+$ has thus far been underestimated for temperatures above 2000 K.

The partition function Q_{all} provides our best estimate. It differs only slightly; the maximum difference is about 0.6 per cent at 5000 K, from Q_{37} which was obtained using only our levels in our final states file, as was our cooling function calculation. Energy states with $J = 38$–40 are absent from the states file as they do not participate in transitions with frequency values less than 25 000 cm^{-1}. The comparison of the partition functions suggests that our line list and cooling function can be regarded as at least 99 per cent complete for temperatures up to 5000 K.

We recommend using our partition function directly and note that simply summing levels in the states file will give incorrect values because of the duplicate low-precision $J = 25$ levels present in this

Table 3. Partition function values, Q, as a function of temperature, T. Q_{NT} are the values of Neale & Tennyson (1995); while Q_J are our values summed up to $J = 20$ and 25 000 cm^{-1}, $J = 25$ and 25 000 cm^{-1}, $J = 37$ and 35 000 cm^{-1} (based on our states file); Q_{all} denotes partition function values obtained using all calculated energy states with J up to 40 and energies up to 42 000 cm^{-1}.

| T (K)	Q_{NT}	Q_{20}	Q_{25}	Q_{37}	Q_{all}
100	7.360	7.397	7.397	7.397	7.397
500	80.579	80.581	80.581	80.581	80.581
1000	245.762	245.774	245.775	245.775	245.775
1400	473.731	473.833	473.875	473.875	473.875
2000	1102.926	1106.588	1108.442	1108.539	1108.539
2400	1808.406	1832.712	1842.438	1843.513	1843.514
3000	3438.088	3623.212	3682.579	3698.207	3698.310
3500	5385.317	6005.538	6186.521	6268.304	6269.639
4000	7870.782	9441.981	9877.496	10 175.791	10 184.991
4500	10 851.290	14 134.011	15 018.507	15 857.630	15 899.213
5000	14 259.164	20 231.616	21 815.767	23 766.140	23 905.737
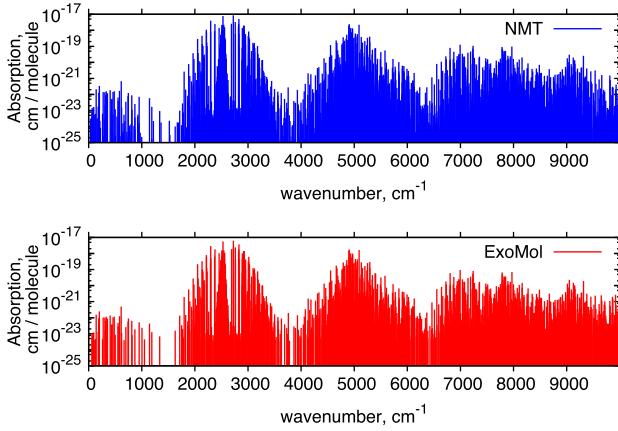
Figure 2. Comparison of MiZATeP line list with the NMT one (Neale et al. 1996) for the room temperature 296 K.
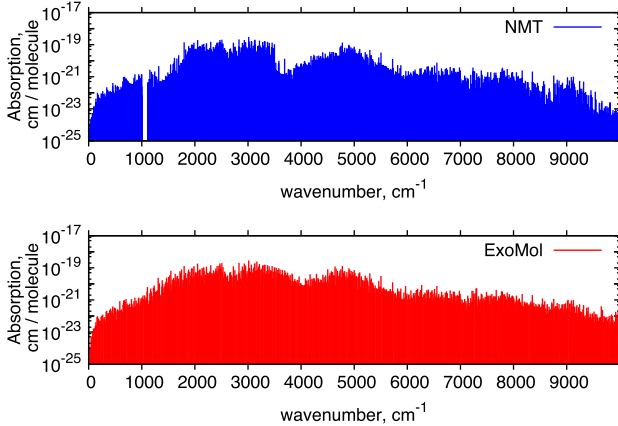

Figure 3. Comparison of MiZATeP line list with the NMT one (Neale et al. 1996) for the temperature value 2500 K.

file. The partition function and cooling function are given in steps of 1 K up to 5000 K in the supplementary material.

Figs 2 and 3 compare the MiZATeP and NMT line lists at room temperature and at 2500 K, respectively, for the frequency range up to 10 000 cm^{-1}. There is generally good agreement although NMT appears to have an unexplained gap in their data between 1000 and
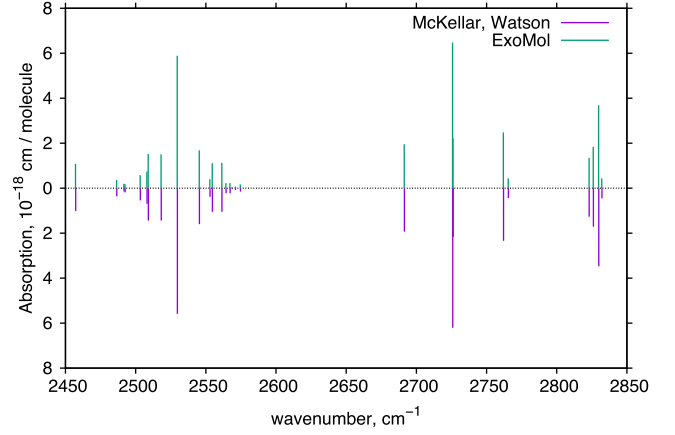
Figure 4. Comparison of calculated spectral lines with the experimental ones obtained by McKellar & Watson (1998). The calculations were performed with the temperature value equal to 285 K.
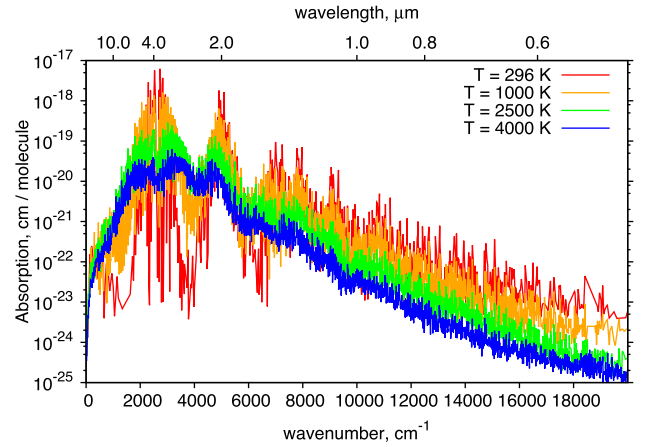
Figure 5. Temperature dependence of MiZATeP line list for H$_3^+$. The curves become increasingly smooth as the temperature increases.

1110 cm^{-1} which is not present in our new calculations. At room temperature the two line lists give similar results, whereas at 2500 K there are obvious differences between them.

We compared the MiZATeP line list with the only available laboratory measurement giving absolute transition intensities, which was performed by McKellar & Watson (1998). To carry out this comparison it was necessary to estimate the temperature of the observed spectrum; a value of 285 K was chosen by inspection of the intensity ratios. Fig. 4 shows the result. The agreement is excellent, with a standard deviation between the calculated intensity values from experiment of about 6 per cent; this difference probably reflects the uncertainty in the assumed temperature and deviations from thermodynamic equilibrium in the experimental sample.

Finally, Fig. 5 illustrates temperature dependence of the MiZATeP line list over a wide temperature range: from room temperature to 4000 K. At the highest temperatures the absorption spectrum becomes much smoother.

5 LIFETIMES AND COOLING FUNCTION CALCULATIONS

Lifetimes of states from the obtained list of energy levels were computed. The algorithm of this calculation was standard

Table 4. Calculated H_3^+ energy states with infinite lifetimes, E_{calc}, together with corresponding energy levels, E_M, obtained during the MARVEL analysis by Furtenbacher et al. (2013).

E_{calc}	E_M	Δ	Sym	v_1	v_2	l_2	J	G	U	K
64.12331	64.121000	50.0	E''	0	0	0	1	1	m	1
86.96619	86.960000	50.0	A_2'	0	0	0	1	0	m	0
315.31645	315.354081	15.2	A_2''	0	0	0	3	3	m	3
995.72428	995.890624	507.8	A_2'	0	0	0	6	6	m	6
1301.93329	1302.142000	10100.0	E''	0	0	0	7	7	m	7
2030.26910	2030.625886	833.3	A_2''	0	0	0	9	9	m	9
2451.10129			E'	0	0	0	10	10	m	10
2856.41347	2856.730003	1111.1	A_2''	0	0	0	10	9	m	9
3402.42821			A_2'	0	0	0	12	12	m	12
3931.31406			E''	0	0	0	13	13	m	13
4449.14478			A_2'	0	0	0	13	12	m	12
5091.29170			A_2''	0	0	0	15	15	m	15
5720.68071			E'	0	0	0	16	16	m	16
6341.32985			A_2''	0	0	0	16	15	m	15
7074.35983			A_2'	0	0	0	18	18	m	18
7797.41071			E''	0	0	0	19	19	m	19
8508.15437			A_2'	0	0	0	19	18	m	18

Notes.

E_{calc}/E_M: Calculated here MARVEL state energy in cm^{-1}.

Δ: Uncertainty of MARVEL energy states in 10^{-6} cm^{-1}.

Sym: Symmetry of the state.

v_1: Symmetric stretch quantum number.

v_2: Bending quantum number.

l_2: Vibrational angular momentum quantum number of the degenerate v_2 mode.

J: Total angular momentum.

K: Absolute value of the projection of J on the C_3.

G: Absolute value of quantum number $g = k - l_2$ (Watson 1984).

U: U-notation of Watson (1984).

(Tennyson et al. 2016a): we obtained a sum of Einstein A coefficients of each transition from our final line list, which includes the given level as an upper one. The inverse value of the calculated sum is the sought-for lifetime of the given state. Lifetimes were only obtained for states for which accurate calculations were available: those with J up to 20 and energies less than 25 000 cm^{-1}.

Our lifetime calculations give an interesting result. Any molecular system possesses a few very long-lived quantum states from which radiative decay is impossible either because of the absence of lower-lying states, or because such transitions are forbidden by selection rules. For example, a recent study on the H_3O^+ system found three such meta-stable states for H_3O^+ and four for D_3O^+ (Melnikov et al. 2016). We find a number of such states for which decay is not possible, all of which belong to the vibrational ground state of the system. Considering states with $J \leq 19$, we find a total 17 stable states for the H_3^+ system, with energies up to 8509 cm^{-1}. These states are listed in Table 4. Only a few (meta-)stable states could be anticipated on symmetry grounds. The other states are stabilized because there are no lower-lying states (generally levels in the $J - 1$ manifold), which are reachable given the rather stringent selection rules in force in H_3^+. These meta-stable states are responsible for the observed astrophysical and laboratory lifetime effects discussed in Introduction.

The MiZATeP line list is given ExoMol format as a states file, see Table 5, and a transitions file, see Table 6. It was used to compute cooling function values for temperatures up to 5000 K. The cooling function is the total energy emitted by a single molecule in one second per unit solid angle. We used the analytical formula given by Tennyson et al. (2016a) and a version of states file with purely

Table 5. Extract from the states file for H_3^+. The full table is available from http://cdsarc.u-strasbg.fr/cgi-bin/VizieR?-source=J/MNRAS/xxx/yy.

i	$\tilde{E}$	g	J	τ	p	Sym	v_1	v_2	l_2	G	U	K
1	0.000000	0	0	NaN	e	A_1'	0	0	0	0	m	0
2	64.121000	6	1	INF	e	E''	0	0	0	1	m	1
3	86.960000	12	1	INF	f	A_2'	0	0	0	0	m	0
4	169.294000	10	2	2.3491E+06	e	E'	0	0	0	2	m	2
5	237.357000	10	2	1.7812E+06	f	E''	0	0	0	1	m	1
6	315.354081	28	3	INF	e	A_2''	0	0	0	3	m	3
7	428.019000	14	3	5.7399E+04	f	E'	0	0	0	2	m	2
8	494.773333	14	3	2.6579E+04	e	E''	0	0	0	1	m	1
9	502.028333	18	4	3.9059E+08	e	E'	0	0	0	4	m	4
10	516.878695	28	4	1.3589E+04	f	A_2'	0	0	0	0	m	0
11	658.722423	36	4	1.6935E+04	f	A_2''	0	0	0	3	m	3
12	729.031652	22	5	6.7686E+09	e	E''	0	0	0	5	m	5
13	768.475373	18	4	5.5360E+03	e	E'	0	0	0	2	m	2
14	833.578848	18	4	1.6480E+03	f	E''	0	0	0	1	m	1
15	928.965633	22	5	4.6803E+04	f	E'	0	0	0	4	m	4
16	995.890624	52	6	INF	e	A_2'	0	0	0	6	m	6
17	1080.490719	44	5	5.5069E+04	e	A_2''	0	0	0	3	m	3
18	1187.117384	22	5	4.9087E+02	f	E'	0	0	0	2	m	2
19	1238.467378	26	6	1.5981E+05	f	E''	0	0	0	5	m	5
20	1250.313955	22	5	3.0108E+02	e	E''	0	0	0	1	m	1

Notes. i: State counting number.

$\tilde{E}$: State energy in cm^{-1}.

g: Total degeneracy of the state.

J: Total angular momentum.

τ: Lifetime of the state. INF means that the given state is meta-stable, and NaN denotes unknown lifetime values of states without accurate labelling.

p: e/f – parity as given by DVR3D (Tennyson et al. 2004).

Sym: Symmetry of the state.

v_1: Symmetric stretch quantum number.

v_2: Bending quantum number.

l_2: Vibrational angular momentum quantum number of the degenerate v_2 mode.

K: Absolute value of the projection of J on the C_3.

G: Absolute value of quantum number $g = k - l_2$ (Watson 1984).

U: U-notation of Watson (1984).

Table 6. Extract from the transitions file for H_3^+. The full table is available from http://cdsarc.u-strasbg.fr/cgi-bin/VizieR?-source=J/MNRAS/xxx/yy.

i	f	A_{if}
55649	55648	1.7919E-16
42887	42882	2.2552E-13
85624	85623	4.3421E-25
88580	88579	1.5729E-22
55549	55548	3.6088E-13
46682	46681	4.3625E-14
62743	62742	3.4064E-14
55021	55017	5.8630E-14
59376	59371	4.7837E-13
31241	31239	1.5502E-12
100507	100506	9.0073E-22
28798	28795	3.3924E-12
82321	82320	1.6180E-20
81287	81282	2.0435E-12
68802	68801	1.9590E-13
98580	98579	3.8420E-20
70437	70436	8.0826E-24
47335	47334	2.8127E-13
80312	80308	6.5889E-15
60950	60949	6.0748E-20

Notes. i: Upper state counting number.

f: Lower state counting number.

A_{if}: Einstein A coefficient in s^{-1}.

Table 7. Cooling function values, W, as a function of temperature, T. W_{Mel} and W_{Mil} are the values of Melin (2006) and Miller et al. (2013), respectively, in units of Watts Molecule^{-1} Steradian^{-1}, while W_{our} are our values, in the same units system, summed up to $J = 37$ and $42\,000$ cm^{-1} (based on our states file).

T (K)	W_{Mel}	W_{Mil}	W_{our}	$\frac{W_{\mathrm{our}}}{W_{\mathrm{Mel}}}$	$\frac{W_{\mathrm{our}}}{W_{\mathrm{Mil}}}$
20			4.43×10^{-32}		
50		3.36×10^{-30}	3.37×10^{-30}		1.003
100		1.29×10^{-28}	1.26×10^{-28}		0.977
150		1.01×10^{-27}	1.03×10^{-27}		1.020
200		1.63×10^{-26}	1.69×10^{-26}		1.037
300		5.35×10^{-24}	5.32×10^{-24}		0.994
500	5.05×10^{-22}	6.77×10^{-22}	6.69×10^{-22}	1.325	0.988
700	4.16×10^{-21}	5.74×10^{-21}	5.52×10^{-21}	1.327	0.962
900	1.41×10^{-20}	2.05×10^{-20}	1.87×10^{-20}	1.326	0.912
1200	4.49×10^{-20}	7.45×10^{-20}	5.95×10^{-20}	1.325	0.799
1500	9.80×10^{-20}	1.92×10^{-19}	1.30×10^{-19}	1.327	0.677
1700	1.47×10^{-19}	3.21×10^{-19}	1.95×10^{-19}	1.327	0.607
1800	1.75×10^{-19}	4.03×10^{-19}	2.33×10^{-19}	1.331	0.578
2000		6.05×10^{-19}	3.20×10^{-19}		0.529
3000		2.16×10^{-18}	9.59×10^{-19}		0.444
4000		3.81×10^{-18}	1.80×10^{-18}		0.472
5000		4.77×10^{-18}	2.63×10^{-18}		0.551

calculated energies (i.e. without replacing them by MARVEL analysis results) to compute the cooling function.

Table 7 gives our cooling function results. It compares them (W_{our}) with values W_{Mel} from Melin (2006) and W_{Mil} from Miller et al. (2013) when possible the cooling curve presented in Melin (2006) is valid only in temperature range from 500 to 1800 K, while the one from Miller et al. (2013) can be calculated for temperature values 30–5000 K. The standard deviation of the ratio of our results to the ones by Melin (2006) is about 33 per cent, while for comparison with Miller et al. (2013) its value is about 43 per cent.

6 CONCLUSION

The MiZATeP full line list can be downloaded from the CDS, via ftp://cdsarc.u-strasbg.fr/pub/cats/J/MNRAS/xxx/yy, or http://cdsarc.u-strasbg.fr/viz-bin/qcat?J/MNRAS//xxx/yy, as well as the exomol website, www.exomol.com. The line lists, cooling and partition functions together with auxiliary data including the potential parameters and dipole moment functions can all be obtained also from www.exomol.com as part of the extended ExoMol data base (Tennyson et al. 2016b).

REFERENCES

Al-Refaie A. F., Yurchenko S. N., Yachmenev A., Tennyson J., 2015, MNRAS, 448, 1704
Al-Refaie A. F., Polyansky O. L. I. R., Ovsyannikov Tennyson J., Yurchenko S. N., 2016, MNRAS, 461, 1012
Asvany O., Hugo E., Schlemmer S., Muller F., Kuhnemann F., Schiller S., Tennyson J., 2007, J. Chem. Phys., 127, 154317
Azzam A. A. A., Yurchenko S. N., Tennyson J., Naumenko O. V., 2016, MNRAS, 460, 4063

Barber R. J., Tennyson J., Harris G. J., Tolchenov R. N., 2006, MNRAS, 368, 1087
Barber R. J., Strange J. K., Hill C., Polyansky O. L., Mellau G. C., Yurchenko S. N., Tennyson J., 2014, MNRAS, 437, 1828
Barton E. J., Yurchenko S. N., Tennyson J., 2013, MNRAS, 434, 1469
Barton E. J., Chiu C., Golpayegani S., Yurchenko S. N., Tennyson J., Frohman D. J., Bernath P. F., 2014, MNRAS, 442, 1821
Bergeron P., Ruiz M. T., Leggett S. K., 1997, ApJS, 108, 339
Brittain S. D., Rettig T., 2002, Nature, 418, 57
Cencek W., Rychlewski J., Jaquet R., Kutzelnigg W., 1998, J. Chem. Phys., 108, 2831
Coppola C. M., Lodi L., Tennyson J., 2011, MNRAS, 415, 487
Dinelli B. M., Polyansky O. L., Tennyson J., 1995, J. Chem. Phys., 103, 10433
Dinelli B. M., Neale L., Polyansky O. L., Tennyson J., 1997, J. Mol. Spectrosc., 181, 142
Diniz L. G., Mohallem J. R., Alijah A., Pavanello M., Adamowicz L., Polyansky O. L., Tennyson J., 2013, Phys. Rev. A, 88, 032506
Drossart P. et al., 1989, Nature, 340, 539
Engel E. A., Doss N., Harris G. J., Tennyson J., 2005, MNRAS, 357, 471
Farnik M., Davis S., Kostin M. A., Polyansky O. L., Tennyson J., Nesbitt D. J., 2002, J. Chem. Phys., 116, 6146
Furtenbacher T., Császár A. G., 2012, J. Quant. Spectrosc. Radiat. Transf., 113, 929
Furtenbacher T., Császár A. G., Tennyson J., 2007, J. Mol. Spectrosc., 245, 115
Furtenbacher T., Szidarovszky T., Matyus E., Fabri C., Csaszar A. G., 2013, J. Chem. Theor. Comput., 9, 5471
Geballe T. R., Oka T., 1996, Nature, 384, 334
Geballe T. R., Jagod M. F., Oka T., 1993, ApJ, 408, L109
Geballe T. R., Goto M., Usuda T., Oka T., McCall B. J., 2006, ApJ, 644, 907
Geballe T. R., Mason R. E., Oka T., 2015, ApJ, 812, 56
Glover S., Savin D. W., 2006, Phil. Trans. R. Soc. A, 364, 3107
Goto M., McCall B. J., Geballe T. R., Usuda T., Kobayashi N., Terada H., Oka T., 2002, PASJ, 54, 951
Goto M., Geballe T. R., McCall B. J., Usuda T., Suto H., Terada H., Kobayashi N., Oka T., 2005, ApJ, 629, 865
Goto M. et al., 2008, ApJ, 688, 306
Harris G. J., Larner F. C., Tennyson J., Kaminsky B. M., Pavlenko Y. V., Jones H. R. A., 2008, MNRAS, 390, 143
Herbst E., Klemperer W., 1973, ApJ, 185, 505
Indriolo N., McCall B. J., 2012, ApJ, 745, 91
Jaquet R., Carrington T., 2013, J. Phys. Chem. A, 117, 9493
Johnson B. R., 1983, J. Chem. Phys., 79, 1916
Kao L., Oka T., Miller S., Tennyson J., 1991, ApJS, 77, 317
Khodachenko M. L., Shaikhislamov I. F., Lammer H., Prokopov P. A., 2015, ApJ, 813, 50
Koskinen T. T., Aylward A. D., Miller S., 2007, Nature, 450, 845
Kreckel H. et al., 2002, Phys. Rev. A, 66, 052509
Kreckel H., Schwalm D., Tennyson J., Wolf A., Zajfman D., 2004, New J. Phys, 6, 151
Kutzelnigg W., Jaquet R., 2006, Phil. Trans. R. Soc. A, 364, 2855
Lam H. A., Achilleos N., Miller S., Tennyson J., Trafton L. M., Geballe T. R., Ballester G. E., 1997a, Icarus, 127, 379
Lam H. A., Miller S., Joseph R. D., Geballe T. R., Trafton L. M., Tennyson J., Ballester G. E., 1997b, ApJ, 474, L73
Lie G. C., Frye D., 1992, J. Chem. Phys., 96, 6784
Lindsay C. M., McCall B. J., 2001, J. Mol. Spectrosc., 210, 60
McCall B. J., Oka T., 2000, Science, 287, 1941
McCall B. J., Geballe T. R., Hinkle K. H., Oka T., 1998, Science, 279, 1910
McCall B. J., Geballe T. R., Hinkle K. H., Oka T., 1999, ApJ, 522, 338
McCall B. J. et al., 2002, ApJ, 567, 391
McCall B. J. et al., 2003, Nature, 422, 500
McKellar A. R. W., Watson J. K. G., 1998, J. Mol. Spectrosc., 191, 215
McKemmish L. K., Yurchenko S. N., Tennyson J., 2016, MNRAS, 463, 771
Melin H., 2006, PhD thesis, University College London

Melnikov V. V., Yurchenko S. N., Tennyson J., Jensen P., 2016, Phys. Chem. Chem. Phys., 18, 26268

Millar T. J., 2015, Plasma Sources Sci. Technol., 24, 043001

Miller S., Tennyson J., 1988a, Chem. Phys. Lett., 145, 117

Miller S., Tennyson J., 1988b, ApJ, 335, 486

Miller S., Tennyson J., Lepp S., Dalgarno A., 1992, Nature, 355, 420

Miller S., Lam H. A., Tennyson J., 1994, Can. J. Phys., 72, 760

Miller S. et al., 1995, Geophys. Res. Lett., 22, 1629

Miller S. et al., 2000, Phil. Trans. R. Soc. Lond. A, 358, 2485

Miller S., Stallard T., Melin H., Tennyson J., 2010, Faraday Discuss., 147, 283

Miller S., Stallard T., Tennyson J., Melin H., 2013, J. Phys. Chem. A, 117, 9633

Moss R. E., 1996, Mol. Phys., 89, 195

Munro J. J., Ramanlal J., Tennyson J., 2005, New J. Phys, 7, 196

Neale L., Tennyson J., 1995, ApJ, 454, L169

Neale L., Miller S., Tennyson J., 1996, ApJ, 464, 516

Oka T., 2006, Proc. Natl. Acad. Sci., 103, 12235

Oka T., 2013, Chem. Rev., 113, 8738

Oka T., Geballe T. R., Goto M., Usuda T., McCall B. J., 2005, ApJ, 632, 882

Pan F. S., Oka T., 1986, ApJ, 305, 518

Patrascu A. T., Tennyson J., Yurchenko S. N., 2015, MNRAS, 449, 3613

Paulose G., Barton E. J., Yurchenko S. N., Tennyson J., 2015, MNRAS, 454, 1931

Pavanello M., Tung W.-C., Leonarski F., Adamowicz L., 2009, J. Chem. Phys., 130, 074105

Pavanello M. et al., 2012a, Phys. Rev. Lett., 108, 023002

Pavanello M. et al., 2012b, J. Chem. Phys., 136, 184303

Pavlyuchko A. I., Yurchenko S. N., Tennyson J., 2015, MNRAS, 452, 1702

Petrignani A. et al., 2014, J. Chem. Phys., 141, 241104

Polyansky O. L., Tennyson J., 1999, J. Chem. Phys., 110, 5056

Polyansky O. L., Dinelli B. M., Le Sueur C. R., Tennyson J., 1995, J. Chem. Phys., 102, 9322

Polyansky O. L., Kyuberis A. A., Lodi L., Tennyson J., Ovsyannikov R. I., Zobov N., 2016, MNRAS, 466, 1363

Polyansky O. L., Kyuberis A. A., Lodi L., Tennyson J., Ovsyannikov R. I., Zobov N., Yurchenko S. N., 2017, MNRAS, preprint (arXiv:e-prints).

Rego D., Achilleos N., Stallard T., Miller S., Prange R., Dougherty M., Joseph R. D., 1999, Nature, 399, 21

Rivlin T., Lodi L., Yurchenko S. N., Tennyson J., Le Roy R. J., 2015, MNRAS, 451, 5153

Röhse R., Kutzelnigg W., Jaquet R., Klopper W., 1994, J. Chem. Phys., 101, 2231

Schiffels P., Alijah A., Hinze J., 2003a, Mol. Phys., 101, 175

Schiffels P., Alijah A., Hinze J., 2003b, Mol. Phys., 101, 175

Schiffels P., Alijah A., Hinze J., 2003c, Mol. Phys., 101, 189

Shkolnik E., Gaidos E., Moskovitz N., 2006, ApJ, 132, 1267

Sochi T., Tennyson J., 2010, MNRAS, 405, 2345

Sousa-Silva C., Hesketh N., Yurchenko S. N., Hill C., Tennyson J., 2014, J. Quant. Spectrosc. Radiat. Transf., 142, 66

Sousa-Silva C., Al-Refaie A. F., Tennyson J., Yurchenko S. N., 2015, MNRAS, 446, 2337

Stallard T., Miller S., Melin H., Lystrup M., Cowley S. W. H., Bunce E. J., Achilleos N., Dougherty M., 2008a, Nature, 453, 1083

Stallard T. et al., 2008b, Nature, 456, 214

Tennyson J., 1993, J. Chem. Phys., 98, 9658

Tennyson J., 1995, Rep. Prog. Phys., 58, 421

Tennyson J., Sutcliffe B. T., 1982, J. Chem. Phys., 77, 4061

Tennyson J., Sutcliffe B. T., 1983, J. Mol. Spectrosc., 101, 71

Tennyson J., Yurchenko S. N., 2012, MNRAS, 425, 21

Tennyson J., Kostin M. A., Barletta P., Harris G. J., Polyansky O. L., Ramanlal J., Zobov N. F., 2004, Comput. Phys. Commun., 163, 85

Tennyson J., Hulme K., Naim O. K., Yurchenko S. N., 2016a, J. Phys. B: At. Mol. Opt. Phys., 49, 044002

Tennyson J. et al., 2016b, J. Mol. Spectrosc., 327, 73

Trafton L. M., Geballe T. R., Miller S., Tennyson J., Ballester G. E., 1993, ApJ, 405, 761

Underwood D. S., Tennyson J., Yurchenko S. N., Huang X., Schwenke D. W., Lee T. J., Clausen S., Fateev A., 2016a, MNRAS, 459, 3890

Underwood D. S., Tennyson J., Yurchenko S. N., Clausen S., Fateev A., 2016b, MNRAS, 462, 4300

Voronin B. A., Tennyson J., Tolchenov R. N., Lugovskoy A. A., Yurchenko S. N., 2010, MNRAS, 402, 492

Watson W. D., 1973, ApJ, 183, L17

Watson J. K. G., 1984, J. Mol. Spectrosc., 103, 350

Whitten R. C., Smith F. T., 1968, J. Math. Phys., 9, 1103

Wolniewicz L., 1988, J. Chem. Phys., 90, 371

Wolniewicz L., Hinze J., Alijah A., 1993, J. Chem. Phys., 99, 2695

Wong A., Yurchenko S. N., Bernath P., Mueller H. S. P., McConkey S., Tennyson J., 2017, MNRAS, preprint (arXiv:e-prints)

Yadin B., Vaness T., Conti P., Hill C., Yurchenko S. N., Tennyson J., 2012, MNRAS, 425, 34

Yorke L., Yurchenko S. N., Lodi L., Tennyson J., 2014, MNRAS, 445, 1383

Yurchenko S. N., Tennyson J., 2014, MNRAS, 440, 1649

Yurchenko S. N., Barber R. J., Tennyson J., 2011, MNRAS, 413, 1828

Yurchenko S. N., Blissett A., Asari U., Vasilios M., Hill C., Tennyson J., 2016, MNRAS, 456, 4524

SUPPORTING INFORMATION

Supplementary data are available at *MNRAS* online.

part+cool_func_list.txt

Please note: Oxford University Press is not responsible for the content or functionality of any supporting materials supplied by the authors. Any queries (other than missing material) should be directed to the corresponding author for the article.

This paper has been typeset from a TeX/LaTeX file prepared by the author.